The composition of EphB2 clusters determines the strength in the cellular repulsion response

Andreas Schaupp,[1] Ola Sabet,[2] Irina Dudanova,[1] Marion Ponserre,[1] Philippe Bastiaens,[2] and Rüdiger Klein[1,3]

[1]Department of Molecules – Signaling – Development, Max Planck Institute of Neurobiology, 82152 Martinsried, Germany
[2]Department of Systemic Cell Biology, Max Planck Institute for Molecular Physiology, 44227 Dortmund, Germany
[3]Munich Cluster for Systems Neurology (SyNergy), 80336 Munich, Germany

Trans interactions of erythropoietin-producing human hepatocellular (Eph) receptors with their membrane-bound ephrin ligands generate higher-order clusters that can form extended signaling arrays. The functional relevance of the cluster size for repulsive signaling is not understood. We used chemical dimerizers and fluorescence anisotropy to generate and visualize specific EphB2 cluster species in living cells. We find that cell collapse responses are induced by small-sized EphB2 clusters, suggesting that extended EphB2 arrays are dispensable and that EphB2 activation follows an ON–OFF switch with EphB2 dimers being inactive and trimers and tetramers being fully functional. Moreover, the strength of the collapse response is determined by the abundance of multimers over dimers within a cluster population: the more dimers are present, the weaker the response. Finally, we show that the C-terminal modules of EphB2 have negative regulatory effects on ephrin-induced clustering. These results shed new light on the mechanism and regulation of EphB2 activation and provide a model on how Eph signaling translates into graded cellular responses.

Introduction

Communication between cells via erythropoietin-producing human hepatocellular (Eph)–ephrin signaling is a common mechanism by which cells coordinate complex morphogenetic processes during development, plasticity, and pathologies such as cancer (Egea and Klein, 2007; Pasquale, 2008; Klein, 2009; Astin et al., 2010). Ephrins are membrane-tethered ligands that bind and activate Eph receptor tyrosine kinases (RTKs) in trans at cell–cell interfaces, but they also have intrinsic signaling capabilities making the Eph–ephrin system a versatile and bidirectional communication system. Typically, Eph–ephrin signaling mediates cell repulsion and sorting, although other responses such as adhesion and directed motility have been described (Marquardt et al., 2005; Rohani et al., 2011; Wang et al., 2011). Ephrins interact with Ephs in a subgroup-specific manner, i.e., EphAs bind to glycosylphosphatidylinositol-anchored ephrinAs and EphBs bind to transmembrane ephrinBs, with few exceptions (Himanen et al., 2004).

An essential aspect of Eph–ephrin signaling is the formation of higher order clusters, a feature that distinguishes Ephs from most other RTKs that are activated by dimerization (Hofman et al., 2010; Lemmon and Schlessinger, 2010). Synthetic dimeric ephrin–Fc fusion proteins are not very effective in eliciting functional signaling (Davis et al., 1994) and are sometimes used in vivo as dominantly interfering agents because they seem to interfere with endogenous ephrin–Eph interactions (Lim et al., 2008). When ephrin–Fc fusion proteins are artificially preclustered, however, they lead to the assembly of larger Eph clusters and efficiently induce Eph signaling (Davis et al., 1994). Crystal structures of the EphA2 ectodomain in complex with ephrinAs revealed the formation of extended signaling arrays, providing further evidence for higher-order clustering (Himanen et al., 2010; Seiradake et al., 2010). More recent structures of EphA4 in complex with ephrinB3 and ephrinA5 revealed smaller clusters with a dimeric or circular arrangement (Seiradake et al., 2013). Cell biological experiments suggested that four ephrin units are effective in initiating biological responses (Stein et al., 1998; Vearing et al., 2005). A comparison between EphA2 and EphA4 suggested that cluster size may

Correspondence to Rüdiger Klein: rklein@neuro.mpg.de

Abbreviations used in this paper: ANOVA, analysis of variance; BF, brightfield; Eph, erythropoietin-producing human hepatocellular; FKBP, FK506 binding protein; FRET, Förster resonance energy transfer; GC, growth cone; mGFP, monomeric GFP; PBM, PDZ binding motif; RTK, receptor tyrosine kinase; SAM, sterile α motif.

The Rockefeller University Press $30.00
J. Cell Biol. Vol. 204 No. 3 409–422
www.jcb.org/cgi/doi/10.1083/jcb.201305037

JCB **409**

be an important determinant of the quality of cellular response (Seiradake et al., 2013).

Interactions of the Eph ectodomain with other Ephs in cis may facilitate clustering (Wimmer-Kleikamp et al., 2004). Interactions of the Eph intracellular domain with other Ephs or interacting proteins may also modulate Eph clustering. Sterile α motif (SAM) domains located at the Eph C terminus may oligomerize and thereby promote clustering (Qiao and Bowie, 2005). The C-terminal PDZ (postsynaptic density-95/discs large/zona occludens-1) binding motif (PBM) mediates coclustering of EphB receptors with AMPA-type glutamate receptors in neurons (Kayser et al., 2006). Other general parameters such as plasma membrane properties (Salaita et al., 2010) may further influence Eph clustering.

Because of the dynamic nature of Eph clustering, it has thus far been impossible to analyze the cellular and biochemical functions of predefined Eph cluster sizes to see what requirements are needed to induce a physiological response. Here, we have used a chemical genetic approach to generate EphB2 clusters of defined sizes in living cells to assess the regulation of EphB2 clustering and the importance of cluster size for EphB2 signaling.

Results

Generation and imaging of EphB2 cluster populations

To generate defined EphB2 clusters in the absence of ephrins, we used a synthetic dimerizer (AP20187) with high binding affinity to a 12-kD mutant FK506 binding protein (FKBP) domain (Clackson et al., 1998), which we inserted together with GFP variants into the EphB2 cytoplasmic region (Fig. 1 A). The insertion of a single FKBP domain leads to the formation of dimers, which previous work showed is sufficient to fully activate most growth factor receptors (Muthuswamy et al., 1999; Whitney et al., 2001), but not EphB2 (see Fig. 3, A–C; and see Fig. 4 A). To generate higher-order clusters, we inserted two or three FKBP domains into EphB2. These modifications shifted the mobility of EphB2 in blue native PAGE (Fig. S1 A; Wittig et al., 2006). Importantly, these modifications did not appear to affect EphB2 signaling properties upon activation with extracellular ephrins, including autophosphorylation, internalization kinetics, and cell collapse responses (see Figs. S3 B and S4, A and B). We also confirmed that the dimerizer-induced EphB2 clusters do not recruit wtEphB2 by performing phosphorylation assays and single cell image analysis (Fig. S1, B–G). To resolve distinct cluster populations, EphB2-FKBP isoforms were transiently expressed in COS7 cells, stimulated with AP20187, and separated with blue native PAGE followed by anti-EphB2 immunoblots (Fig. 1 B, density plot). Stimulation of cells expressing the 1FKBP isoform resulted in the formation of dimers with residual amounts of monomers. Binding of AP20187 to 2FKBP isoforms resulted in the formation of EphB2 oligomers. Although dimers were still abundant, trimers became the predominant form, and oligomers up to pentamers could be distinguished. The presence of three FKBP domains shifted the cluster composition toward larger oligomers; dimers were rather rare (Fig. 1 B). These results indicate that chemical dimerizers can produce distinct EphB2 cluster populations in living cells.

To visualize the degree of EphB2 clustering in single cells, we used Förster resonance energy transfer (FRET) between identical fluorophores (homo-FRET), previously used to study membrane protein clustering and receptor oligomerization (Varma and Mayor, 1998; Hofman et al., 2010). Homo-FRET concerns nonradiative energy transfer between similar fluorophores within nanometer distance and results in a decrease of the steady-state fluorescence anisotropy of the fluorophore (Runnels and Scarlata, 1995). We inserted a monomeric GFP (mGFP) in our 1–3FKBP EphB2 constructs to assess the level of oligomerization of the different Eph variants. An inverse correlation is expected between cluster size and anisotropy because of the extended Förster energy migration within larger clusters of mGFP that lower the anisotropy. Using epifluorescent anisotropy imaging, we found that the initial anisotropy value of mGFP in all receptor-FKBP variants was similar across different fluorescence intensities except for very low levels, where anisotropy tailed off because of cellular background fluorescence contributions (Fig. 1 C). Addition of AP20187 decreased anisotropy in all cases (Fig. 1 C) with saturation at 20 min for all FKBP isoforms (Video 1 and Fig. S2 A). The decrease in anisotropy correlated with the number of FKBP domains with an initial, large decrease observed when EphB2 formed dimers (Fig. 1 C). Quantification of fluorescence anisotropy was done at the periphery of the cell that represented mostly receptors in the plasma membrane as opposed to the center where the signals originate from receptors in endomembranes.

After having determined the relative abundance of monomers, dimers, and multimers (Fig. 1 B) in the cluster populations of different FKBP constructs, we were able to estimate the relative contributions of these different association states to a given anisotropy value. We plotted the distribution of anisotropy values from the periphery of multiple cells (see Materials and methods) that express a given FKBP construct incubated with the dimerizer. The mean molecular brightness of each state to the total intensity was used as a weighing factor in computing the relative contribution of each association state to anisotropy (Fig. 1 D). This allowed us to clearly distinguish three association states and their corresponding anisotropy values. First, there was a monomeric state shared by all FKBP constructs before dimerization with an anisotropy value of $A_M \pm$ std. = 0.278 ± 0.009. Second, there was a dimeric state obtained after dimerizing the 1FKBP construct with an anisotropy value of $A_D \pm$ std. = 0.237 ± 0.011. Third, there was a mixture of oligomeric association states of trimers and higher-order clusters with an anisotropy value of $A_O \pm$ std. = 0.218 ± 0.013. Because dimerizer-induced EphB2 oligomers are functional (see Fig. 4 A), we assumed that they are structurally similar to ephrin-induced oligomers. We therefore used the calculated anisotropy values to estimate the complexity of EphB2 cluster populations at sites of contact between ephrinB2[+] and EphB2^{+} cells. Cells expressing kinase-dead EphB2 tagged with mGFP (kdEphB2-mGFP) were co-cultured with cells expressing ephrinB2 (tagged with mCherry) and sites of ephrinB–EphB interactions were visualized by colocalization of the two fluorophores (Fig. 2, A–C).
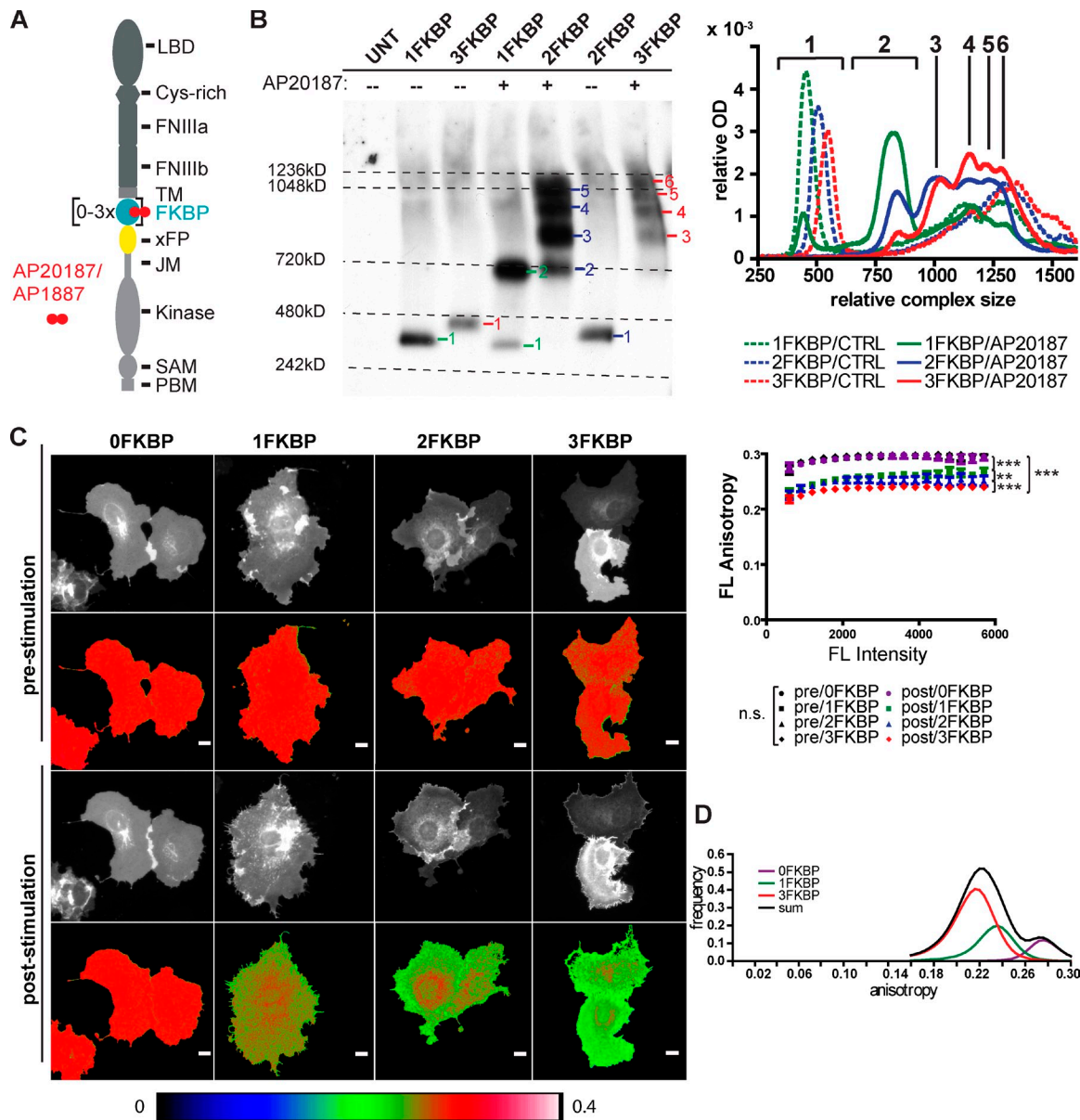
Figure 1. **Generation and imaging of EphB2 cluster populations.** (A) Domain structure of EphB2/A4 with 1 to 3FKBP domains and a single fluorescent protein (xFP indicates different variants of GFP) inserted in the cytoplasmic tail close to the transmembrane domain. Homodimerizers AP20187 (IC_{50} = 1.8 nM) or AP1887 (IC_{50} = 40 nM) noncovalently cross-link FKBP domains of neighboring Eph receptors. FNIII, fibronectin type III domain; JM, juxtamembrane; LBD, ligand-binding domain; TM, transmembrane; xFP, spectral variant of GFP. (B) AP20187-induced cluster sizes of kinase-dead EphB2-FKBP-mGFP isoforms visualized by blue native PAGE (UNT, untransfected). KdEphB2 was used to avoid rapid internalization. Note that EphB2 migrates as a much larger protein compared with denaturing conditions and small shifts in molecular mass are in accordance with the number of FKBP domains inserted (see Fig. S1 A). (right) An incremental mean optical density lane scan gives the distribution patterns with peaks indicating single resolvable cluster species. Incremented mean optical density was normalized to the sum over all increments. Representative experiment of n = 4. (C) Steady-state fluorescence anisotropy of dimerizer-induced EphB2 clusters in living cells. COS-7 cells transiently expressing kdEphB2 with different numbers of FKBP domains fused to mGFP were stimulated with 250 nM AP20187. Anisotropy values of representative cells before and 20 min after stimulation with AP20187 are shown. Bars, 20 µm. The color coding of images is shown on the bottom. The graph on the right shows anisotropy plots before and after stimulation of 0 to 3FKBP isoforms. Data represent mean anisotropy ± SEM of n = 57, 28, 22, and 20 cells from n = 3 independent experiments for 3FKBP, 2FKBP, 1FKBP, and 0FKBP integrated over whole frame, respectively. Post-stimulation curves of 0–3FKBP are all significantly different from each other and controls. (0/1FKBP, 0/2FKBP, 0/3FKBP, 1/3FKBP, and 2/3FKBP: ***, P < 0.001; 1/2FKBP: **, P < 0.01; Mann-Whitney nonparametric test). (D) The graph shows the intensity-weighted distribution of anisotropy values for the different association states. Data were extracted in ImageJ from raw eroded after dimerization anisotropy images (erosion = 10–15 pixels) for 0FKBP (n = 20 cells), 1FKBP (n = 22 cells), and 3FKBP (n = 57 cells) from n = 3 independent experiments. 0FKBP was used to represent the monomeric state (purple trace), 1FKBP the dimeric state (green trace), and 3FKBP the multimeric state (red trace). Summed anisotropy distributions (black trace) were later used for calculation of each association state contribution to a given anisotropy value.

Kinase-dead EphB2 was used to prevent endocytosis of the receptors (Zimmer et al., 2003), a process that likely influences clustering dynamics. Fluorescence anisotropy imaging revealed focal areas of very low anisotropy, indicative of higher-order

EphB2 clustering (Fig. 2 D). The intensity-weighted distribution of anisotropy values (Fig. 1 D) was used to map the cumulative relative contribution of each association state for a given anisotropy value (Fig. 2 E). A map of the contribution of each
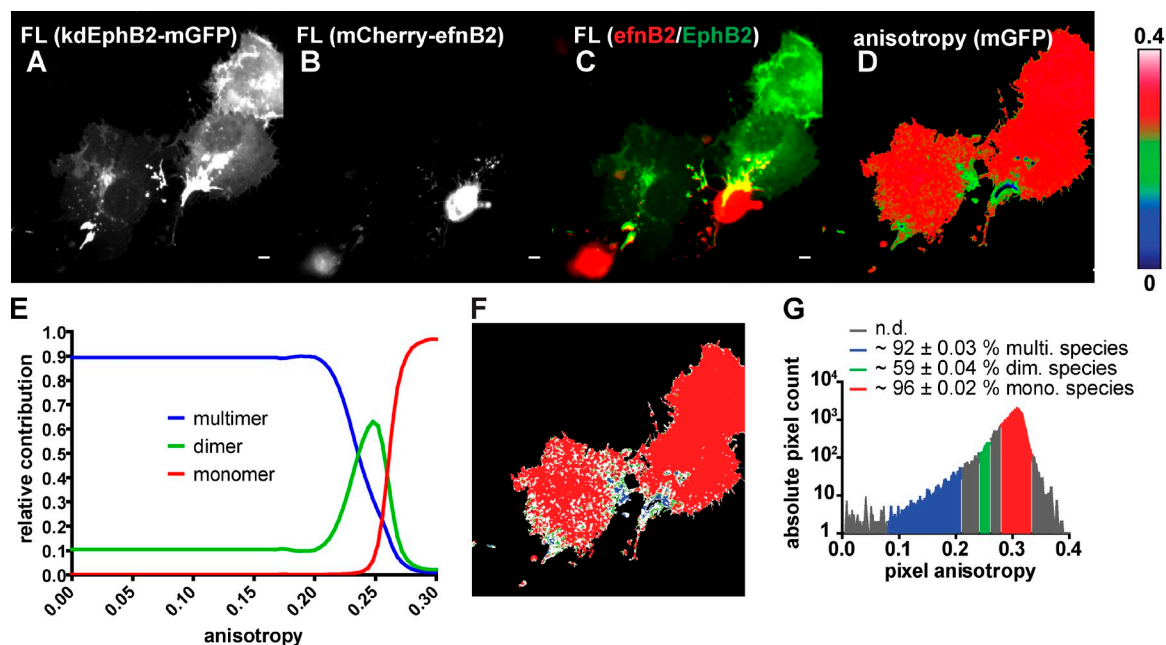
Figure 2. **Fluorescence anisotropy analysis of EphB2 clusters at contacts with ephrinB2-expressing cells.** Nonuniform clustering response of kdEphB2 upon contact with ephrinB2-expressing cells. COS-7 cells transiently transfected with kdEphB2-mGFP (A) were co-cultured with HEK293 cells stably expressing wild-type mCherry-ephrinB2 (B; merged image in C). Homo-FRET between kdEphB2-mGFP was determined by fluorescence anisotropy (D). Representative experiment from a series of co-cultures (n = 20 cells analyzed). (E) For calibration of anisotropy values to cluster size distributions the cumulative relative contributions of 0FKBP (monomer, n = 20 cells), 1FKBP (dimer, n = 22 cells), and 3FKBP (oligomer, n = 57 cells) from n = 3 independent experiments were plotted to the range of anisotropy values on the x-axis (see Materials and methods). (F) Areas with color coded and calibrated anisotropy pixel distributions of predominantly monomers, dimers, and multimers according to the histogram (G). Contact areas in which the anisotropy values were too low to be quantified (because of intensity saturation) are shown in black pixels. Bars, 10 µm.

association state was computed from the anisotropy image of ephrinB2⁺/EphB2⁺ cell co-cultures (Fig. 2, F and G). This allowed us to observe distinct areas with multimers surrounded by distinct areas of mostly dimers at ephrinB–EphB contact sites (Fig. 2, F and G). These results indicate that EphB2/ephrinB cluster populations at cell–cell interfaces are heterogeneous, raising the possibility that the degree of heterogeneity may modulate cellular responses.

Degree of EphB2 clustering determines strength of kinase activity

Next, we investigated if the composition of the EphB2 cluster population determined the strength of EphB2 signaling. Upon AP20187 stimulation, we found a positive correlation between the numbers of inserted FKBP domains (i.e., the mean size of the EphB2 oligomeric state) and EphB2 autophosphorylation, both by immunofluorescence of single cells (Fig. S2, B and C) and by immunoblotting (Fig. S3, A–C). To determine the relative contributions of different EphB2 oligomeric species to the total autophosphorylation levels, we separated them using blue native PAGE (Fig. 3 A). Cumulative relative autophosphorylation of all EphB2 cluster species showed again significant stepwise increases from the 1 to 3FKBP isoforms (Fig. 3 B). There was a small difference in phosphorylation of trimers and larger oligomers between cells expressing 2 or 3FKBP, but this difference was not significant (Fig. 3 C). Instead, relative to the phosphorylation of dimers, phosphorylation of trimers and larger oligomers was twofold higher in cells expressing 2 or 3FKBP isoforms. Moreover, the ratio between monomers/dimers and oligomers

differed between the 2 and 3FKBP isoforms: whereas the ratio was 1:3 in cells expressing the 2FKBP isoforms, it became 1:10 in cells expressing the 3FKBP isoforms (Fig. 3 D and Fig. S3 D). Because of the higher abundance of hypophosphorylated dimers, we hypothesized that the 2FKBP isoform would be less potent in inducing signaling than the 3FKBP isoform because the cumulative signaling response of the total receptor pool is the sum of its oligomeric species. To test this directly, we measured the phosphorylation of an Eph substrate in living cells, an assay that we had previously established for the related EphA4 receptor (Egea et al., 2005) that also binds ephrinB ligands (Gale et al., 1996). EphA4-2FKBP and EphA4-3FKBP isoforms had similar clustering and autophosphorylation properties as EphB2 (Fig. S3 E). In support of our hypothesis, dimerizer-induced clustering of the 3FKBP isoform caused stronger substrate phosphorylation than the 2FKBP isoform (Fig. S3 F). In contrast, substrate phosphorylation induced by ephrinB3-Fc was similar for both isoforms (Fig. S3 F). Together these findings suggest that the relative abundance of multimers and dimers within an EphB2 cluster population determines the strength of Eph kinase activity.

Degree of Eph clustering determines strength of cellular response

Next we asked if the composition of EphB2 cluster populations also correlated with the strength of cell responses. The application of soluble active forms of ephrins typically results in a collapse response of transfected cells or neuronal growth cones (GCs) expressing the corresponding Eph receptors. We found that, qualitatively, dimerizer-induced and ephrinB2-Fc–induced
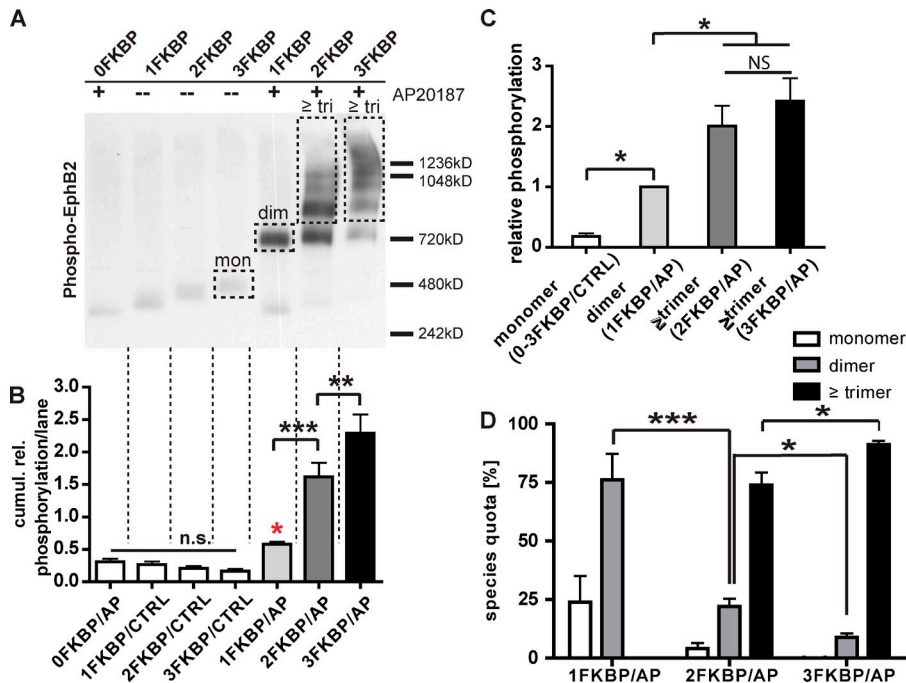
Figure 3. **Degree of Eph clustering determines receptor activation.** (A) Representative blue native PAGE blot for autophosphorylation analysis of single EphB2 oligomeric species (B–D). Blue native PAGE of lysates of COS-7 cells expressing different FKBP isoforms of wtEphB2 and stimulated with either vehicle (−) or AP20187 (250 nM for 20 min). Western blot was performed with anti-phospho-EphB2 antibodies; blots were stripped and reblotted for total EphB2 protein (see Fig. S3 D). The relative phosphorylation levels of single oligomeric species were measured according to example regions outlined by dashed boxes for monomers, dimers, and species greater than or equal to trimers. (B) Quantification of the cumulative relative phosphorylation per lane displayed as mean ratio ± SEM of phosphorylated versus total EphB2 protein over $n = 4$ blue native PAGE experiments (*, $P < 0.05$; **, $P < 0.01$; ***, $P < 0.001$; one-way ANOVA with post hoc Bonferroni test; asterisk in red represents significance level to 1FKBP control stimulation). (C) Quantitative autophosphorylation analysis of single cluster species displayed as mean ratio ± SEM of phosphorylated versus total EphB2 protein from example regions in A from $n = 4$ blue native PAGE experiments normalized to dimer phosphorylation level set to 1.0 (*, $P < 0.05$, one-way ANOVA with post hoc Bonferroni test). (D) Relative abundance of cluster species in percentage ± SEM of cumulated species population (*, $P < 0.05$; ***, $P < 0.001$; Student's t test). Data are derived from optical density quantification of regions outlined by dashed boxes in A on Western blots for total EphB2 (see Fig. S3 D) of $n = 4$ blue native PAGE experiments.

clustering of EphB2 (containing 3FKBP domains) resulted in similar EphB2 (or EphA4) internalization and cell collapse responses (Video 2 and Fig. S4, A–C). As expected from the autophosphorylation analysis, EphB2 dimers produced very minor cell contractions (Fig. 4 A). In contrast, cells expressing the 2 and 3FKBP isoforms responded to AP20187 with pronounced cell collapse (Fig. 4 A). Importantly, cells expressing the 3FKBP isoform showed significantly stronger cell collapse compared with the 2FKBP, both in terms of kinetics and degree of cell contraction (Fig. 4 A). These results indicate that dimerizer-induced EphB2 clustering is sufficient to cause cellular responses and that the degree of EphB2 clustering positively correlates with strength of the response.

Next, we used a low affinity dimerizer (AP1887; Clackson et al., 1998) to produce clusters with reduced internal stability to mimic interaction of EphB2 with lower affinity ephrins. The cluster size distribution was of similar complexity as for AP20187 (unpublished data), but the kinetics of EphB2 autophosphorylation was much slower than for AP20187, eventually reaching similar levels (Fig. 4 B). The low affinity, dimerizer-induced cell collapse response was slower and less pronounced compared with AP20187 (Fig. 4 C). The response curve showed remarkable similarity to that obtained with the low affinity ligand ephrinA5-Fc (Himanen et al., 2004), which also induced a weaker cell collapse than the high affinity ligands ephrinB2-Fc and ephrinB3-Fc (Fig. 4 D). These results suggest that the stability of EphB2 clusters also determines the strength of the cellular response.

To further test the functional relevance of our findings, we asked if dimerizer-induced EphB2 clusters were able to trigger GC collapse in neurons (Egea et al., 2005). We overexpressed wtEphB2 carrying three FKBP domains in primary rat hippocampal neurons and measured dimerizer-induced GC collapse. We used EphB2 isoforms lacking most of the ectodomain including the ephrin ligand binding domain (ΔNEphB2) to avoid interference with endogenous ephrins (Fig. S5, A and B). Before the addition of AP20187, neurons expressing ΔNEphB2-3FKBP or expressing ΔNEphB2 lacking FKBP domains were indistinguishable from neurons transfected with a control YFP plasmid (Fig. 5 A). However, addition of AP20187 caused GC collapse of neurons expressing the 3FKBP isoform, but not the 0FKBP isoform, to a similar extent as bath-applied, preclustered ephrinB2-Fc (Fig. 5, A and B). The low affinity dimerizer AP1887 had a reduced effect compared with AP20187, but still significantly increased the fraction of collapsed GCs (Fig. 5 B). These results indicate that dimerizer-induced EphB2 clusters elicit physiological responses in neurons with response characteristics remarkably similar to ephrin-induced EphB2 clusters.

Synergy between intra- and extracellular clustering determinants

After having compared the association between EphB2 clustering and the resulting responses, we next investigated the regulation of EphB2 clustering in living cells. We asked whether clustering induced by extracellular ephrins would be modulated by clustering determinants engaging the EphB2 intracellular domain. As proof of principle we took advantage of the fact that FKBP domains can be used in a bifunctional way to either activate or inhibit clustering (see the following paragraph). To explore the synergy between extra- and intracellular clustering, we overexpressed EphB2 carrying a single FKBP domain in cells and costimulated with the homodimerizer AP20187 and/or sub-threshold doses of unclustered ephrinB2-Fc (Fig. 6 A).
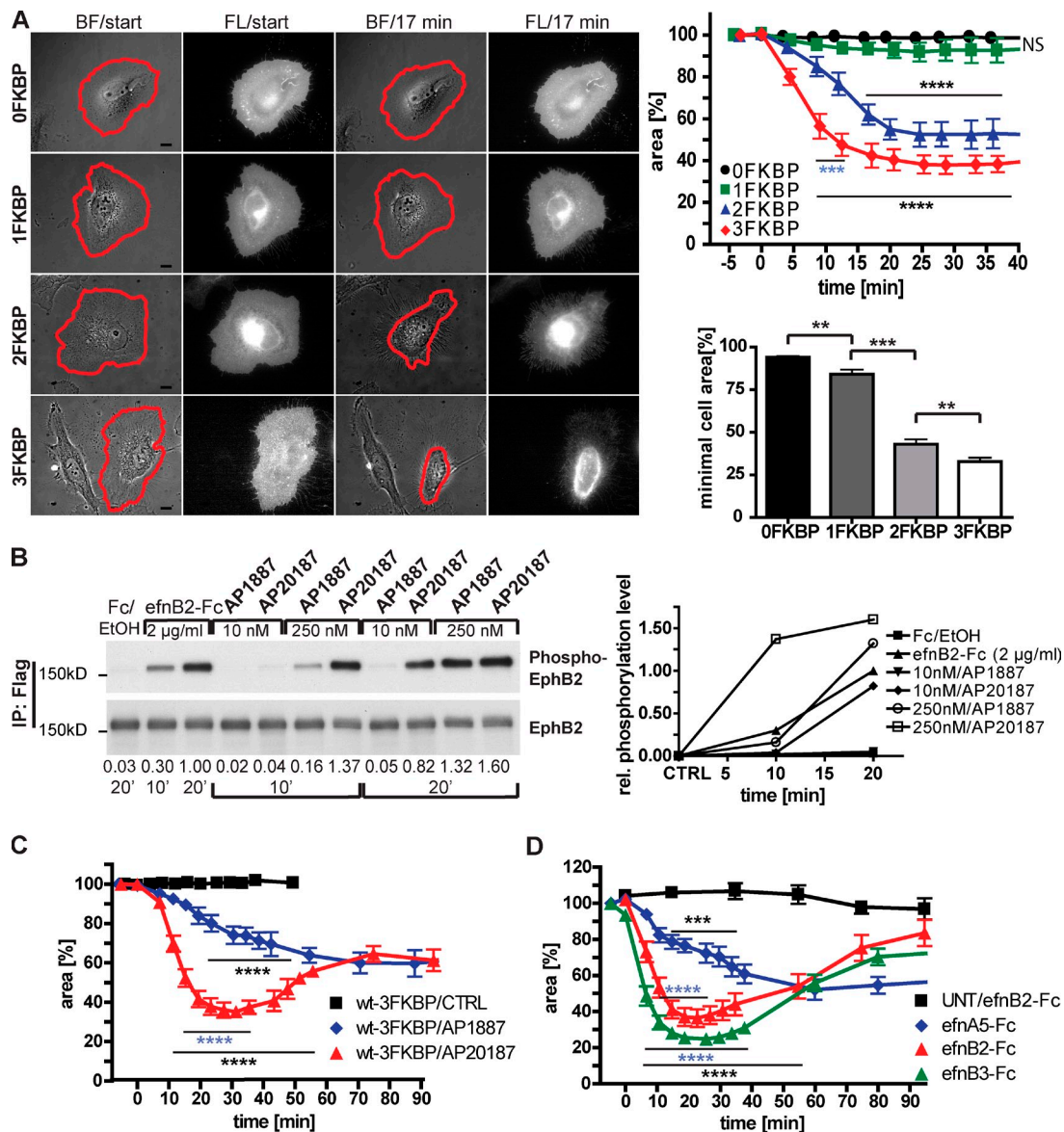
Figure 4. **Degree of EphB2 clustering determines strength of cellular response.** (A) Images of representative HeLa cells in bright-field (BF) and fluorescence, expressing equal and moderate levels of wtEphB2 carrying 0 to 3FKBP domains, before (start) and after stimulation with 250 nM AP20187 for 17 min. Cell collapse was scored by measuring the cell surface area (red outlines; see Materials and methods). (top right) Graph showing changes in mean cell area (± SEM from n = 10 cells for each isoform) over time (in percentage relative to the start of the experiment) induced by AP20187. Statistical significance was determined using two-way ANOVA with post hoc Bonferroni test and is shown with black stars (0 versus 2 or 3FKBP) and blue stars (2 versus 3FKBP); ***, P < 0.001; ****, P < 0.0001. (bottom right) Bar graph showing changes in collapse amplitude (minimal surface area in percentage relative to start of experiment) of cells within 40 min after stimulation (mean cell area ± SEM from n = 30 cells for each isoform; **, P < 0.01; ***, P < 0.001, Student's t test). Bars, 10 µm. (B) Representative Western blot of anti-Flag immunoprecipitated EphB2-3FKBP isoforms using anti-phospho-EphB2 antibodies; blots were stripped and reblotted for total EphB2 levels. Blots show the time course of EphB2 autophosphorylation in transfected HeLa cells induced by the low-affinity dimerizer AP1887, compared with the indicated concentrations of high-affinity dimerizer AP20187, or preclustered ephrinB2-Fc. Note that the kinetics of EphB2 autophosphorylation was slower for AP1887 compared with AP20187. After 20 min, 250 nM AP1887 was as effective as AP20187 and ephrinB2-Fc. In total the experiment was repeated three times with the same outcome. (C) Quantification of collapse responses of cells expressing the wtEphB2-3FKBP isoform induced by the low affinity dimerizer AP1887 compared with AP20187 (each 250 mM; mean cell area ± SEM from n = 17, 16, and 12 cells for conditions AP20187, AP1887, and control). Statistical significance was determined as in A and is shown with black stars (control versus dimerizer) and blue stars (AP1887 versus AP20187). Note that the response induced by AP1887 is slower and weaker. (D) Quantification of collapse responses of cells expressing wtEphB2 induced by equal concentrations (2 µg/ml) of preclustered ephrinB2-Fc and ephrinB3-Fc compared with the low affinity ligand ephrinA5-Fc. As a control, cell collapse of untransfected cells (UNT) was measured upon ephrinB2-Fc stimulation (mean cell area ± SEM from n = 13, 14, 15, and 8 cells for conditions ephrinB2-Fc, ephrinB3-Fc, ephrinA5-Fc, and UNT/ephrinB2-Fc) Statistical significance was determined as in A and is shown with black stars (untransfected versus wtEphB2) and blue stars (ephrinA5-Fc versus ephrinB2-Fc or ephrinB3-Fc).

Intracellular dimerization by AP20187 alone caused a 2.35-fold higher autophosphorylation of EphB2, whereas low doses of unclustered ephrinB2-Fc had no effect (Fig. 6 B). Interestingly, costimulation with AP20187 and ephrinB2-Fc had synergistic effects on EphB2 activation and cell collapse (Fig. 6, B and C; and Fig. S5 C).

To inhibit clustering, we induced the association of EphB2 with a membrane-tethered FKBP-associated protein
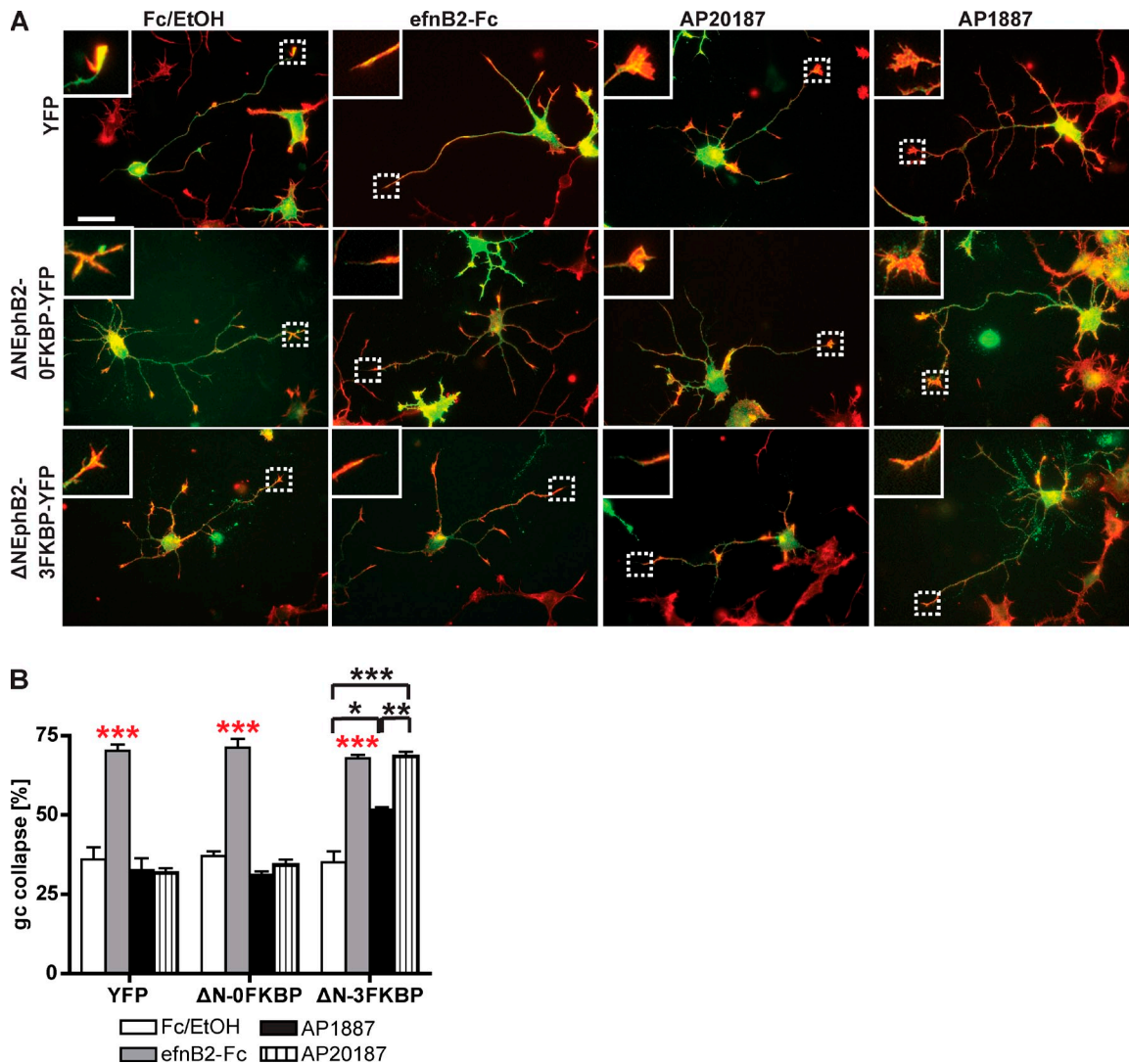
Figure 5. **Dimerizer-induced EphB2 clusters cause GC collapse in neurons.** (A) Rat hippocampal cultures were transfected with YFP, ΔNEphB2-0FKBP, or ΔNEphB2-3FKBP, and treated at 1 d in vitro with control stimuli (Fc fragment plus ethanol), 1 µg/ml preclustered ephrinB2-Fc, 250 nM AP20187, or 250 nM AP1887 for 30 min. Neurons were fixed and stained with anti-GFP antibody (green) and phalloidin (red) to visualize f-actin–rich GCs. Insets show GCs indicated by dashed boxes. Only the status of GCs of the longest neurites positive for Tau1 (axons) was quantified. Bar: (main images) 30 µm; (insets) 10 µm. (B) Quantification of GC collapse (mean ± SEM in percentage of all GCs counted). EphrinB2-Fc induced GC collapse in all cultures. AP20187 was as efficient as ephrinB2-Fc in inducing GC collapse in neurons expressing the 3FKBP isoform, whereas stimulation with AP1887 led to an intermediate response ($n = 3$ independent experiments; ***, $P < 0.001$; **, $P < 0.01$; *, $P < 0.05$; Student's t test; asterisks in red represent significance level to Fc/EtOH control stimulation of each dataset).

(myrFRB-mCherry) by stimulating the cells with a high-affinity heterodimerizer (AP21967; Chen et al., 1995; Choi et al., 1996; Fig. 6 D). The presence of the heterodimerizer AP21967 prevented ephrinB2-Fc from inducing EphB2 clustering, autophosphorylation, and cell collapse (Fig. 6, E and F; and Fig. S5 D). The heterodimerizer also changed Eph-ephrin signaling in a cell–cell stimulation assay. Under control conditions, EphB2 clusters that emerged at the contact site between the two opposing cells were internalized into the cells and triggered the typical repulsion response (Zimmer et al., 2003; Fig. 7, A and C). In the presence of the heterodimerizer, however, EphB2 clusters remained static at the cell edges without being processed, and cell repulsion was absent or very weak (Fig. 7, B and C). Hence, intracellular inhibition of EphB2 clustering converted repulsion to adhesion, whereas intracellular enhancement of EphB2 clustering strengthened the collapse response.

Next we asked if the presence of the SAM domain and PBM in the EphB2 intracellular domain would influence EphB2 clustering. SAM/PBM may bind scaffolding or adaptor protein complexes that positively or negatively regulate clustering, e.g., by steric hindrance. We compared the clustering properties of wtEphB2-mGFP with an EphB2 deletion mutant lacking both SAM domain and PBM (EphB2ΔSAM/PBM) by fluorescence anisotropy imaging in COS-7 cells. In the absence of ephrinB2-Fc, the degree of EphB2 clustering was low, independently of the presence of SAM domain and PBM (Fig. 8, A and B). Upon stimulation with unclustered ephrinB2-Fc, some degree of EphB2 clustering was induced and this effect was significantly enhanced in cells expressing mutant EphB2ΔSAM/PBM (Fig. 8, A and B), suggesting that SAM/PBM negatively influenced EphB2 clustering. To test if the change in EphB2 clustering translated into

Figure 6. Intracellular clustering determinants sensitize or desensitize cells toward extracellular ephrinB2. (A) Model showing possible synergistic response between extracellular (ephrinB2-Fc) and intracellular (dimerizer) clustering determinants. EphB2-1FKBP forms dimers in the presence of AP20187. Both ephrin ligand and AP20187 together can induce functional oligomers. (B) Western blots of anti-Flag–immunoprecipitated EphB2-1FKBP overexpressed in HeLa cells using anti-phospho-EphB2 antibodies; blot was stripped and reblotted for total EphB2. Cells were stimulated with control (ethanol) or AP20187 (250 nM), in the absence or presence of 5 ng/ml (+) or 10 ng/ml (++) unclustered ephrinB2-Fc for 10 min. Numbers below the blots indicate fold change in phosphorylation compared with Fc/ethanol control (1.0), normalized to total receptor protein levels (representative blot of three experiments). (C) Quantification of collapse responses of cells expressing low levels of the 1FKBP isoform induced by the indicated combinations of stimuli (as in B; for description of the assay see Fig. 4 A; mean cell area ± SEM from n = 8–11 cells per condition; Statistical significance was determined as in Fig. 4 A. Green stars, dimerizer alone versus dimerizer plus ephrinB2-Fc; **, P < 0.01. (D) Model showing intracellular steric hindrance (using myr-FRB-mCherry) of extracellular (ephrinB2-Fc–induced) clustering. In the presence of heterodimerizers AP21967 the coexpressed inhibitory construct myr-FRB-mCherry couples to the wtEphB2-3FKBP receptor, keeping it as monomer. EphrinB2-Fc can still bind to the ectodomain of the receptor.

(E) Western blot of immunoprecipitated wtEphB2-3FKBP (carrying a Flag epitope tag) using the phospho-specific anti-EphB2 antibody; blot was stripped and reblotted for total EphB2. HeLa cells transfected with both wtEphB2-3FKBP and myr-FRB-mCherry were stimulated with ephrinB2-Fc in the presence or absence of AP21967 (representative blot of two separate experiments). (F) Quantification of cell collapse assays. The presence of AP21967 prevents EphB2-3FKBP–transfected cells from collapse in response to ephrinB2-Fc. Mean cell area ± SEM from n = 9 cells per condition tested; P < 0.001, Mann-Whitney nonparametric test.
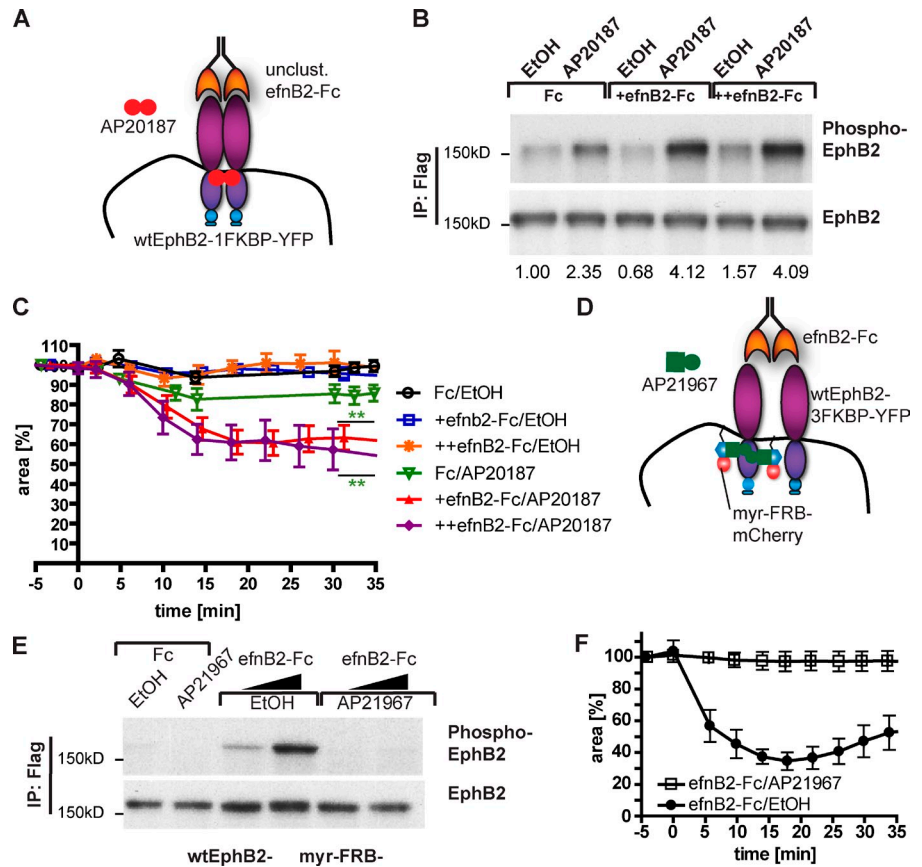
altered signaling and cellular response, we compared wild-type and mutant EphB2 for their autophosphorylation and cell rounding activities. In line with the increased clustering, we found that EphB2ΔSAM/PBM showed significantly increased autophosphorylation compared with wtEphB2 specifically after ephrinB2-Fc stimulation (Fig. 8 C). Moreover, EphB2ΔSAM/PBM was more effective in mediating cellular collapse when expressed at comparable levels as wtEphB2 (Fig. 8, D and E). Together these results indicate that the intracellular domain of EphB2 significantly influences EphB2 clustering and that SAM domain and PBM have a negative impact on EphB2 clustering, thereby putting a break on EphB2 signaling.

Discussion

In this study we used chemical dimerizers to generate different oligomeric states of EphB2 receptors in living cells and analyzed their biochemical and physiological properties. We made three important observations: (1) small-sized EphB2 clusters (trimers and tetramers) produce functional cell responses, an unexpected finding in light of the propensity of EphA2 to form large signaling arrays; (2) EphB2 activation follows an ON–OFF mechanism, suggesting a model in which the relative abundance of active multimers over inactive dimers determines the strength of EphB2

signaling; and (3) the C-terminal SAM domain and PDZ target site of the intracellular domain of EphB2 reduce EphB2 clustering in the presence of extracellular ephrins, an unexpected result in light of propensity of SAM domains to oligomerize (Fig. 9).

Crystal structures of EphA2 ectodomain bound to ephrinAs (Himanen et al., 2010; Seiradake et al., 2010) suggested that Eph/ephrin clusters form large two-dimensional signaling arrays by lateral expansion (Janes et al., 2012). However, a functional analysis of different oligomeric states of Ephs in living cells has been difficult, in part because of the dynamic nature of the clustering process (Wimmer-Kleikamp et al., 2004; Salaita et al., 2010). Here we have used different FKBP isoforms of EphB2 to generate dimers (1FKBP), mostly small-sized clusters (2FKBP) or larger clusters (3FKBP). Our comparison of the activation states of larger oligomers (trimers up to hexamers) in the cluster populations generated by the 2FKP and 3FKBP isoforms did not reveal differences between the two cluster populations (Fig. 3 C), suggesting that small-sized clusters (trimers/tetramers) are already fully activated and that the presence of larger clusters (pentamers, hexamers, etc.) does not enhance the overall signaling activity. How can these results on EphB2 be reconciled with the large arrays observed in EphA2 crystals? A possible explanation is offered by the crystal structure of the related EphA4 receptor whose ectodomain appears to form smaller clusters than EphA2
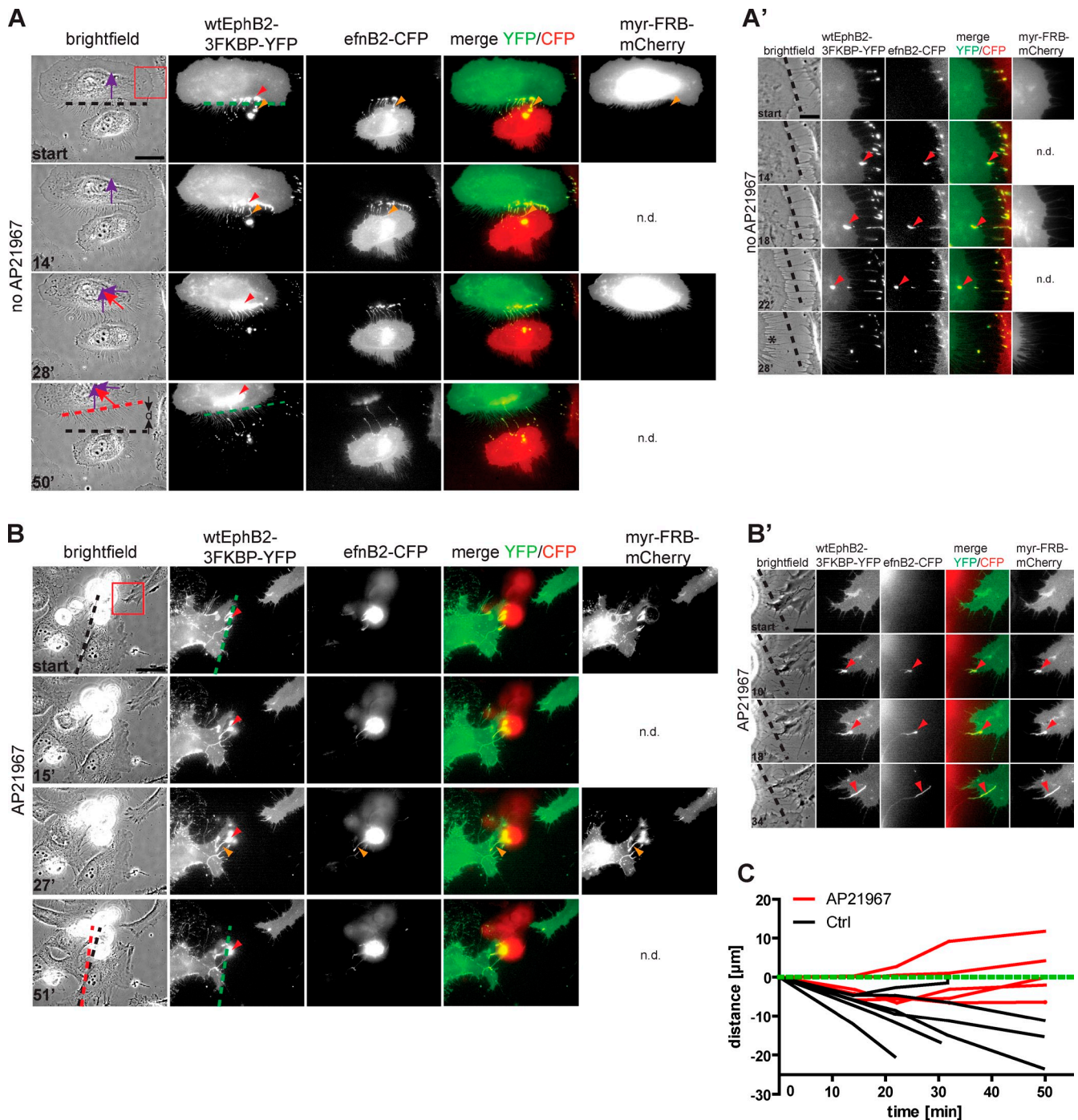
Figure 7. **Inhibition of EphB2 clustering blocks repulsion.** (A and B) Co-culture assay of HeLa cells coexpressing wtEphB2-3FKBP-YFP and a membrane-tethered FKBP-associated protein (myr-FRB-mCherry) with HeLa cells expressing wild-type ephrinB2-CFP in the absence (A) or presence (B) of hetero-dimerizer AP21967. Red box in BF images at starting time point indicates the regions highlighted in the high power images (A′ and B′). EphB2 clusters (red arrowheads) in the contact region of the two cells are turned over in control condition, while remaining static in the presence of the heterodimer-izer. Orange arrowheads indicate colocalization of YFP-EphB2 and CFP-ephrinB2. In the presence of heterodimerizer, myr-FRB-mCherry coclusters with EphB2 (B′). Black dotted lines in first and last BF images indicate original position of EphB2+ cell. Purple arrows in BF images indicate the direction of retraction movements of the EphB2+ cell (first stimulated from below and later from the right) away from two ephrinB2+ cells. Red arrow indicates the di-rection the EphB2 cells moves into. The letter d indicates distance between cells as compared with their initial positions. Red dotted line in last BF image indicates final position of EphB2+ cell. In the presence of the heterodimerizer, adhesion cables form between cells (B′) and retraction is blocked (B). Bars: (A and B) 20 µm; (A′ and B′) 10 µm; n.d., image not taken. (C) Quantification of cell repulsion of EphB2-cells. At time point 0, EphB2+ cell posi-tion was set to 0 (as indicated in A) and was used as a reference for the following time points. Distance to reference border is plotted for each time point. Movement in negative micrometers reflects movement away from the ephrin+ cell. Each line represents a separate cell pair from $n = 2$ different time-lapse experiments. Quantification was done blindly with reference to heterodimerizer stimulation.

Figure 8. C-terminal modules of EphB2 have a negative regulatory effect on ephrinB2-induced clustering. (A) Steady-state fluorescence anisotropy of ephrinB2-induced EphB2 clusters. COS-7 cells transiently expressing wtEphB2-mGFP or EphB2ΔSAM/PBM-mGFP were treated with 0.5 µg/ml unclustered ephrinB2-Fc. Anisotropy values of representative cells before (left) and 20 min after (right) stimulation with ephrinB2 are shown. Deletion of SAM and PBM domains leads to a decrease of fluorescence anisotropy (i.e., increase in clustering). Bars, 10 µM. The color coding of anisotropy values is shown on the right. (B) Quantification of steady-state fluorescence anisotropy plots from before and after stimulation (20 min) with 0.5 µg/ml of unclustered ephrinB2-Fc. Data represent mean anisotropy ± SEM of $n = 35$ and 46 cells for wtEphB2-mGFP and EphB2ΔSAM/PBM-mGFP, respectively. Post-stimulation curves are significantly different from each other; ***, $P < 0.001$; Mann-Whitney nonparametric test. (C, top) Representative Western blots of anti-Flag–immunoprecipitated wtEphB2 or EphB2ΔSAM/PBM (as indicated) after stimulation with equal concentration of Fc control or ephrinB2-Fc (0.5 µg/ml; $t = 20$ min) using mouse anti-phosphotyrosine antibody; blots were stripped and reblotted for total EphB2 protein levels. (bottom) Quantification of autophosphorylation (**, $P < 0.01$; ***, $P < 0.001$; unpaired t test; $n = 7$ separate experiments). (D) Quantification of collapse responses of HeLa cells expressing either wtEphB2 or EphB2ΔSAM/PBM induced by equal concentrations of unclustered human-Fc or ephrinB2-Fc (1 µg/ml is shown; similar results were obtained with 0.5 µg/ml). Cell collapse was scored by measuring cell surface area. Data are shown as mean cell area ± SEM from $n = 25$ cells per condition. Statistical significance was determined as in Fig. 4 A. *, $P < 0.05$; ***, $P < 0.001$; ****, $P < 0.0001$ (wtEphB2 versus EphB2ΔSAM/PBM; $n = 8$ separate experiments). (E) Quantification of EphB2 surface proteins by immunostaining of individual wtEphB2 ($n = 15$ cells) and EphB2ΔSAM/PBM ($n = 15$ cells) transfected cells. Cells were fixed and stained with mouse anti-Flag antibody to visualize EphB2 expressed at cell membranes. Total EphB2 protein levels were visualized by YFP fluorescence. Ratios of surface/total fluorescence intensity integrated over the whole cell body were measured as an indication for expression levels at the cell surface. Scatter in range of EphB2 expression at the cell surface was similar for both conditions with a slight trend toward lower EphB2 level for EphB2ΔSAM/PBM-transfected cells. The experiment was repeated three times with the same outcome.
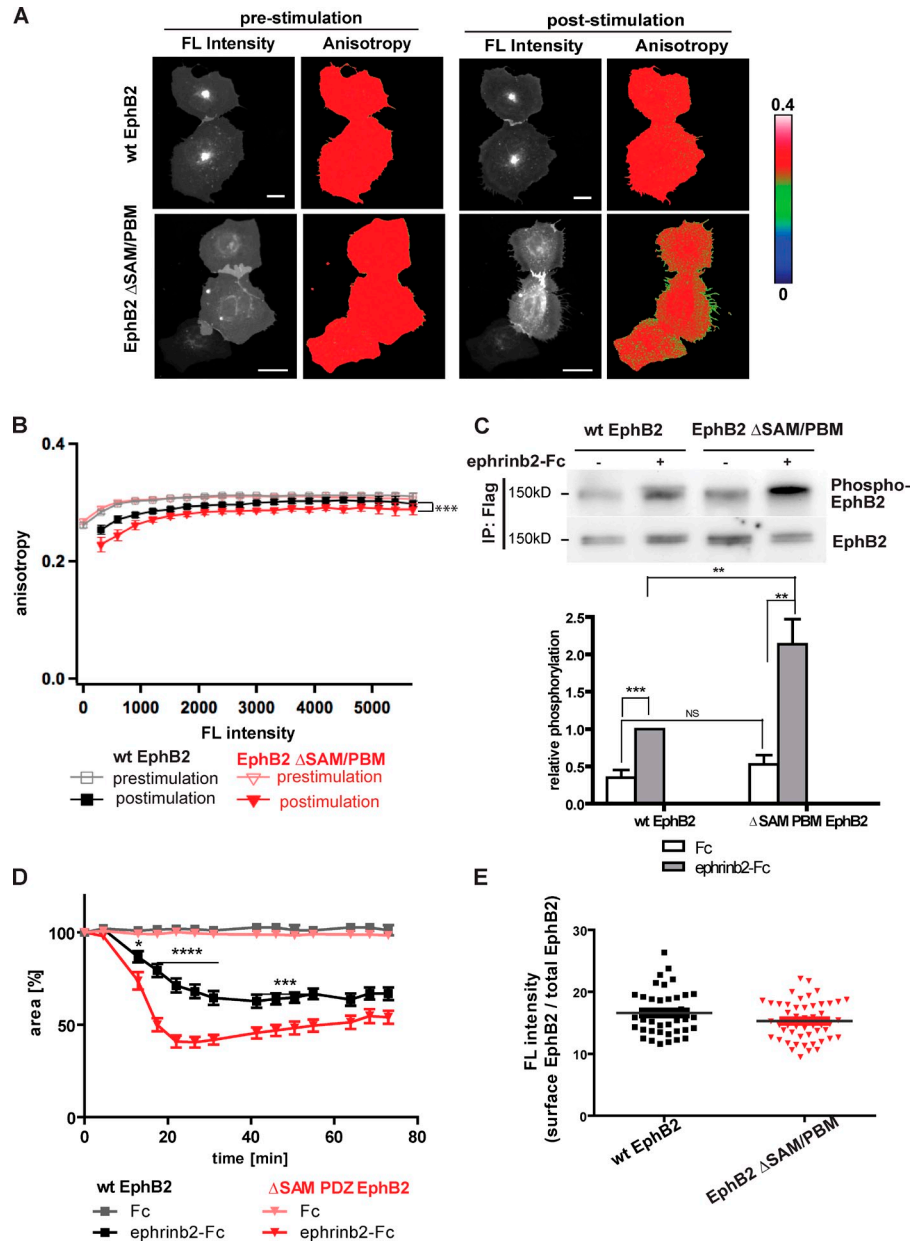
when complexed with ephrins (Seiradake et al., 2013). Moreover, in the response to the same ephrin isoform, EphA4 clusters correlate with cell collapse, whereas EphA2 clusters correlate with adhesive responses, indicating that differences in Eph clusters can drive distinct cell responses. EphB2 that resembles EphA4 in its repulsive signaling output may form similar clusters as EphA4.

These results further suggest that EphB2 activation follows a similar ON–OFF mechanism as other RTKs. Although activation of RTKs by growth factors generally occurs during transition from monomers to dimers (Lemmon and Schlessinger, 2010), the activation switch of EphB2 (and EphA4) receptors occurs during transition from dimers to trimers/tetramers. How could such an ON–OFF mechanism generate graded responses that are necessary

for topographic mapping? The most obvious difference between the two EphB2-FKBP cluster populations was the relative ratio between inactive states (monomers/dimers) and active states (trimers or greater). Whereas the ratio between inactive and active states was 1:3 in cells expressing the 2FKBP isoforms, it became 1:10 in cells expressing the 3FKBP isoforms (Fig. 3 D). We therefore propose that the strength of the cellular response is determined by the relative abundance of higher-order oligomers versus monomers/dimers within EphB2 cluster populations, and not by the shift from small-sized clusters to larger signaling arrays. Consistent with such a model, we find that physiological ephrinB–EphB interactions at cell contact sites are heterogeneous, consisting of dimers and multimers (Fig. 2). Mechanistically,
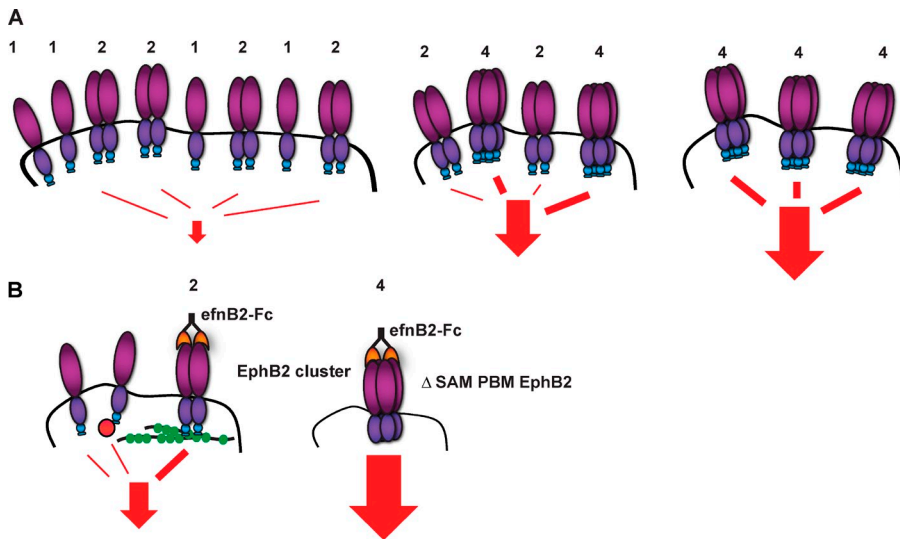
Figure 9. **Model depicting regulation of EphB2 clustering.** (A) EphB2 cluster populations are heterogeneous and the abundance of monomers, dimers, and multimers (only tetramers are shown) determines the strength of the cellular response. A mixture of monomers and dimers is essentially inactive because dimers have weak signaling output. A mixture of dimers and multimers leads to a physiological response; however, the response gets stronger when all dimers are converted to multimers. (B) C-Terminal modules of EphB2 have a negative regulatory effect on ephrinB2-induced clustering, possibly by recruiting unknown interacting proteins and by steric hindrance. Deletion of these modules relieves this inhibitory effect and enhances EphB2 clustering and signaling.

we speculate that cluster populations that consist of predominantly higher-order oligomers will fully phosphorylate and activate the pool of effector proteins in contrast to cluster populations with a significant proportion of inactive states.

The molecular details underlying the activation switch from dimers to trimers/tetramers are currently not clear. It is possible that Ephs are autoinhibited by more than one mechanism and that oligomerization is required to fully relieve autoinhibition. Alternatively, because Eph activation is the result of dynamic sampling of catalytically competent conformations of the kinase domain (Wybenga-Groot et al., 2001; Wiesner et al., 2006), in bigger or more stable clusters the Eph intracellular domain may spend more time in the active conformation and produce stronger signaling output. A molecular crowding effect that limits the spatial freedom of each receptor molecule may be responsible for a shift in the conformational steady-state equilibrium as described by others (Dong et al., 2010). Alternatively, phosphorylated residues of receptors in the center of the cluster may be protected from tyrosine phosphatases that could also contribute to an overall stronger activity of the cluster. To obtain more insights into the dynamics of Eph activation in clusters, Eph kinase sensors will have to be developed.

Finally, we provide direct evidence that the intracellular domain of EphB2 affects oligomerization, which alters the sensitivity of the cells toward extracellular ephrins. We showed that deletion of SAM domain and PDZ target site in EphB2 enhanced EphB2 clustering and signaling. This is contrary to what one may have expected based on previous work on the isolated SAM domain (which showed oligomerization) and on PDZ domain interactions (which were interpreted as positively influencing Eph/ephrin signaling; Qiao and Bowie, 2005; Kayser et al., 2006). The effect of the deletion was only visible under conditions of ephrin stimulation, suggesting the following model: when ephrinBs bind EphB2 and initiate clustering, cytoplasmic proteins are recruited via SAM and PDZ domain associations and these interactions limit EphB2 clustering (by steric hindrance or protein modifications). Freeing EphB2 from these interactions (as in the EphB2ΔSAM/PBM mutant) enhances clustering and signaling. The identity of the interacting proteins that limit EphB2

clustering is currently unknown and will require further work. Moreover, the EphB2ΔSAM/PBM mutant has not been tested for activity in vivo. Interestingly, a similar deletion mutant of EphA4 retained full activity in a *Xenopus laevis* morphogenesis assay, and a conserved tyrosine in the SAM domain was proposed as a protein–protein interaction site for a negative regulator (Park et al., 2004). We demonstrated that EphB2 monomerization blocked ephrinB2-induced cell collapse and retraction in a cell–cell stimulation assay. This observation offers a mechanistic explanation for a switch from repulsive to adhesive cellular responses by steric spacing of receptor monomers as accomplished in cells coexpressing truncated EphA7 splice forms or ephrins (Holmberg et al., 2000; Carvalho et al., 2006). Together these findings shed new light on the mechanisms of Eph activation and signaling and suggest that Eph clustering is a central integrator to elicit graded cellular responses.

Materials and methods

Ethics statement
All animal experiments were conducted in accordance with federal guidelines.

Expression constructs
Expression constructs encoding murine full-length, C-terminally truncated, and kinase-deficient (K660R mutation) EphB2-YFP have been described previously (Zimmer et al., 2003) and served as starting plasmids for insertion of one to three FKBP domains downstream of the transmembrane region from plasmids pC4-FV1E (1FKBP domain), pC4M-FV2E (two FKBP domains; both from Ariad Pharmaceuticals), or pC4M-FV3E (3FKBP domains; insertion of one FKBP domain into pC4M-FV2E via the XbaI–SpeI restriction sites). Constructs wtEphA4-[2,3]FKBP-YFP were obtained by insertion of a PCR-amplified fragment of [2,3]FKBP-YFP into wtEphA4, at the respective site as for EphB2. Different fluorescent protein variants were obtained by excision replacement of EYFP (=YFP) for ECFP (=CFP) from pECFP-N1, mGFP carrying the A206K mutation from pEGFP-N1 (CLONTECH), and mCherry from pRSET-B-mCherry (a gift from R. Tsien, University of California, San Diego, San Diego, CA). The flanking amino acid sequence for insertions in the juxtamembrane region is GFERADSE-[1–3FKBP]-SRDPPVAT-[xFP]-YTDKLQHY. For the C-terminally truncated EphB2-3FKBP construct the remaining EphB2 cytoplasmic domain is GFERADSE followed by three FKBP repeats and YFP. For cloning of the N-terminally truncated ΔNEphB2-[0,3]FKBP expression construct, a cDNA segment was designed and synthesized (MWG Biotech) comprising the fibronectin type III, transmembrane, and part of the juxtamembrane domain. The DNA

fragment was ligated into wtEphB2-[0,3]FKBP-YFP to produce the respective N-terminally truncated versions. The JMA4-GST construct was generated by subcloning a PCR product including the juxtamembrane tyrosines of the mouse EphA4 (sequence RSKY . . . CVAI) in frame with the GST into the bacteria expression vector pGEX-2T (Egea et al., 2005). Expression construct encoding mCherry-HA-ephrinB2 was obtained by excision replacement of CFP by mCherry from CFP-HA-ephrinB2 (Lauterbach and Klein, 2006). To generate myrFRB-mCherry, pC4-RHE (containing the FRB domain fragment; Ariad Pharmaceuticals) served as backbone for insertion of the myristoylation signal and mCherry. All constructs were sequence verified and tested for correct expression.

Reagents and stimulations
Homo- and heterodimerizing agents AP20187 (Clackson et al., 1998), AP1887 (Yang et al., 2003), and AP21967 were obtained from Ariad Pharmaceuticals. Before stimulation, dimerizers were diluted in starving medium used for stimulation to the concentration indicated in the figures. Human IgG Fc fragment (Jackson ImmunoResearch Laboratories, Inc.), mouse ephrinB2-Fc, human ephrinB3-Fc, and human ephrinA5-Fc fusion proteins (R&D Systems) were used for stimulations. For preclustering Fc fragment and ephrin–Fc, fusion proteins were incubated with goat anti–human Fc at a ratio of 5:1 for 30 min at RT.

Antibodies
Primary antibodies used were as follows: rabbit anti-phospho-EphB1/2 Y594/Y604 (Abcam); mouse anti-phosphotyrosine (clone 4G10), mouse anti-FLAG M2 (Sigma-Aldrich); rabbit SAM domain–specific anti-EphB2 (Grunwald et al., 2001); rabbit anti-GST (Santa Cruz Biotechnology, Inc.); rabbit anti-FKBP12 (Thermo Fisher Scientific); mouse monoclonal anti–α-Tubulin (Sigma-Aldrich); mouse monoclonal anti-EphA4/Sek (BD); mouse monoclonal anti-GFP JL-8 (Takara Bio Inc.); rabbit anti-GFP (Invitrogen), 1:2,000; mouse monoclonal anti-Tau1 (EMD Millipore), 1:500, and goat anti–human IgG Fcγ fragment specific for clustering of Fc fusion proteins (Jackson ImmunoResearch Laboratories, Inc.). Secondary antibodies used were as follows: donkey anti–mouse Cy3 or Cy5 conjugated, anti–rabbit Cy2 conjugated, and anti-rabbit/anti-mouse HRP conjugated (Jackson ImmunoResearch Laboratories, Inc.).

Cell culture and transfections
COS-7 cells used for homo-FRET experiments, immunostainings, and blue native PAGE were transfected using FUGENE6 (Roche). HeLa cells were transfected using a Calcium-Phosphate transfection kit (Invitrogen) according to the manufacturer's protocol. 12–16 h before stimulation, cells were starved in growth medium containing dialyzed 0.5% fetal bovine serum (HyClone). For FKBP domain–containing constructs FK506 (300 nM) was added to the growth medium after transfection to reduce Eph clustering.

Primary hippocampal neurons were dissected from embryonic day 18.5 rat embryos, plated onto glass coverslips (Marienfeld) coated with 1 mg/ml poly-D-lysine (Sigma-Aldrich) and 5 µg/ml laminin (Invitrogen), and cultured in Neurobasal-B27 medium (Invitrogen; Lauterbach and Klein, 2006). Neurons were transfected using Amaxa nucleofection kit (Lonza).

Cell culture assays
For cell collapse assays, HeLa cells were detached from the flask using D-PBS lacking Ca^{2+} and Mg^{2+} (Sigma-Aldrich) supplemented with 3 mM EDTA. After washing twice in D-PBS containing Ca^{2+} and Mg^{2+}, cells were seeded in Lab-Tek glass chambers (Thermo Fisher Scientific) coated with 1 mg/ml poly-D-lysine (Sigma-Aldrich) and 5 µg/ml mouse laminin (Invitrogen). 1 h before the start of the experiment, cells were washed with D-PBS and imaging medium DMEM without phenol red supplemented with 25 mM Hepes (Invitrogen).

Immunoprecipitations and Western blotting
Immunoprecipitations from HeLa cells were done as described previously (Egea et al., 2005). Cell lysates were cleared by centrifugation and equal amounts were incubated with 40 µl of anti-FLAG M2-Agarose resin (Sigma-Aldrich) overnight at 4°C, washed four times with lysis buffer, and then analyzed by Western blot. Membranes were incubated overnight with the respective primary antibody, followed by incubation with the species-specific secondary HRP-coupled antibody, and proteins were detected with an enhanced chemiluminescence kit (GE Healthcare). For reblotting, membranes were stripped for 15 min with stripping buffer (Thermo Fisher Scientific) at RT, again blocked with BSA, and reblotted using a primary antibody.

In the kinase-activity assay, coexpressed kinase substrate GST-JMA4 was pulled down with glutathione sepharose 4B (GE Healthcare), and then eluted with loading buffer and subjected to SDS-PAGE for Western blotting. Quantifications of unsaturated Western blots were done using Gel-Pro Analyzer software (Media Cybernetics) normalizing to controls.

Blue native PAGE
COS-7 cells were lysed in NativePAGE sample buffer (Invitrogen) supplemented with 1% n-dodecyl-β-D-maltoside and complete protease and phosphatase inhibitor cocktail (Roche). After centrifugation for 30 min at 13,000 g, equal amounts of cell lysates and a NativeMark unstained protein standard (Invitrogen) were subjected to a 3–12% NativePAGE gradient gel (Invitrogen) in NativePAGE G-250 sample buffer (final concentration 0.25%; Invitrogen). Proteins were then transferred to PVDF membrane and autophosphorylation was detected. For reblotting, membranes were stripped, again blocked with BSA, and reblotted using a primary antibody for total protein detection.

For analysis of cluster sizes the blot was scanned lane by lane using a mean optical density line scan with equal scan width (MetaMorph; Molecular Devices).

For analysis of single cluster phosphorylation, we measured the integrated optical density of the total protein blot and the respective phosphorylation blot from lanes and regions boxing single species (MetaMorph). Relative phosphorylation values from different experiments were normalized to the ratio (phosphorylated/total) of the dimer species (1FKBP) set to 1.0.

Immunocytochemistry
Cells were fixed with prewarmed 2% paraformaldehyde and 4% sucrose in D-PBS for 5 min at RT, rinsed twice with ice cold D-PBS, and then incubated with ice cold 50 mM ammonium chloride in D-PBS for 10 min and rinsed again. For phosphorylation labeling of Eph receptors, cells were permeabilized for 5 min with ice cold 0.1% Triton X-100 in D-PBS at 4°C. For surface labeling of Eph receptors, cells were not permeabilized. Blocking was performed for 30 min at RT or overnight at 4°C with 5% donkey serum (Jackson ImmunoResearch Laboratories, Inc.) and 3% BSA in PBS. Primary antibodies were applied for 60 min at RT. After washing, coverslips were mounted using the ProLong antifade kit (Molecular Probes) or Aqua-Poly/Mount (Polysciences).

Neuronal cultures were fixed with warm 4% paraformaldehyde and 8% sucrose, permeabilized with 0.1% Triton X-100 for 5 min, and incubated with blocking solution (4% goat serum, 4% donkey serum, and 2% BSA in PBS) for 1 h at RT, followed by incubation with the primary antibodies in blocking solution for 2 h at RT. After washing with PBS secondary antibodies diluted 1:250 in blocking solution were applied for 1 h at RT. Texas red–conjugated phalloidin (1:100) was applied together with the secondary antibodies. Coverslips were mounted with fluorescent mounting medium (Dako).

Anisotropy microscopy
Anisotropy microscopy was done in transiently transfected COS-7 cells in DMEM (PAN Biotech) at RT as described by Squire et al. (2004). In brief, images were acquired 15–24 h after transfection, using an inverted microscope (IX81; Olympus) equipped with a MT20 illumination system. A linear dichroic polarizer (Meadowlark Optics) was placed in the illumination path of the microscope, and two identical polarizers were placed in an external filter wheel at orientations parallel and perpendicular to the polarization of the excitation light. The fluorescence was collected via a 20×/0.7 NA air objective, and parallel and polarized emission images were acquired sequentially on an Orca CCD camera (Hamamatsu Photonics). Data acquisition was controlled by the CellR software supplied by the microscope manufacturer. Data processing was done as described previously (Squire et al., 2004) to calculate the steady-state anisotropy in each pixel of the image. For each anisotropy measurement two images were taken: an image with the emission polarizer oriented parallel to the excitation polarizer ($I_{\parallel}$), and one with the emission polarizer oriented perpendicular to the excitation polarizer ($I_{\perp}$). After correcting for shifts between the $I_{\parallel}$ and $I_{\perp}$ images and subtracting the mean background intensity, the steady-state anisotropy was then calculated in each pixel i by:

$$r^i = \frac{G^i I_{\parallel}^i - I_{\perp}^i}{G^i I_{\parallel}^i + 2I_{\perp}^i}.$$

The G factor G^i accounts for differences in sensitivity of the system for the two emission polarization orientations, and was determined by acquiring the ratio of the intensities at parallel and perpendicular orientations. For displaying calculated anisotropy images, we used ImageJ to set the threshold as indicated in figures by numbers on color coding bar.

To determine the cluster size distribution, two binary masks were created, one covered the whole area of a given cell and the other covered an eroded version of the same cell (10–15 pixels removed from the 8-bit binary mask). Subtraction of the second mask from the first created a new binary mask that represents the periphery of the cell that was multiplied

with the original anisotropy image. The distribution of anisotropy values for a given FKBP construct as obtained from multiple samples incubated with the AP20187 dimerizer was then plotted (Fig. 1 C). The mean molecular brightness of each state was used as a weighing factor in computing the relative contribution of each association state to the anisotropy (Fig. 2 E). This intensity-weighted contribution of each association state was divided by their summed anisotropy (Fig. 1 D, black trace), to give the cumulative relative contribution of each association state to a given anisotropy value (Fig. 2 E).

Epifluorescent and confocal imaging

Time-lapse epifluorescence imaging was performed using a Axiovert 200M microscope or an Axioobserver Z1 (Carl Zeiss) equipped with a temperature-controlled carbon dioxide incubation chamber set to 37°C, 65% humidity, and 5% CO_2. Single focal planes were acquired with a 40× phase-contrast objective (Carl Zeiss). For high-resolution epifluorescent live-cell recordings 100×/1.4 NA Plan-Apochromat oil objective (Carl Zeiss) was used with a z-stack resolution of 0.267 µm in fast acquisition mode. Illumination was provided by an X-Cite lamp (series 120; Lumen Dynamics Group) and images were recorded by a Coolsnap HQ camera (Photometrics). Sequential images were acquired using MetaMorph software every 3 to 4 min after addition of the stimulus.

For confocal time-lapse recordings (Video 2), a Fluoview FV1000 confocal microscope (Olympus) equipped with an Argon ion laser (Melles Griot) and a temperature-controlled CO_2 incubation chamber (EMBL) at 37°C was used. Either a 60×/1.2 NA water UPlanSApo or a 60×/1.35 NA oil UPlasSApo objective (Olympus) was used. Images were recorded using Fluoview v. 4.0b (Olympus) software.

Fixed samples were imaged with either a confocal SP2 (Leica) using Leica software or the epifluorescent microscopes Axiovert 200M or Axio Observer Z1 using MetaMorph software.

Image processing

Images were processed using MetaMorph or ImageJ software. Z-stacks of images were corrected for optical density and subjected to adaptive psf blind deconvolution (AutoQuantX; Media Cybernetics) followed by sum or maximum intensity projection as indicated in the figures. For cell collapse quantification, cell edges of montaged stacks were drawn using a tablet pen (Intous 4; Wacom) and MetaMorph software. Cell surfaces of all time points were normalized to the prestimulation image cell surface (set to 100%).

For immunofluorescence, quantification of fluorescence signals was done by measuring the integrated fluorescence intensities from surface or phosphorylation staining from regions or whole cells and normalized to the total protein fluorescence signals. Very high or very low expressing cells were excluded from the analysis as indicated in figure legends.

Statistical analysis

Results are expressed as the means ± SEM. Statistical analysis was performed using Prism (GraphPad Software) or IGOR Pro (WaveMetrics). Statistical tests include the Mann-Whitney nonparametric test, one-way analysis of variance (ANOVA) with post hoc Bonferroni/Tukey-Kramer test, or unpaired Student's *t* test used appropriately as indicated in figure legends. All datasets passed the Kolmogorov and Smirnov test for Gaussian distribution.

Online supplemental material

Fig. S1 shows that overexpressed wild-type and FKBP-containing EphB2 isoforms in lysates of HeLa and COS-7 cells migrate similarly in blue native PAGE, in spite of higher levels of endogenous Eph expression in COS-7 cells, and that endogenous EphB2 receptors are not recruited into dimerizer-induced EphB2-FKBP clusters. Fig. S2 shows that cells transfected with EphB2 receptors carrying different numbers of FKBP domains have different fluorescence anisotropy values and EphB2 autophosphorylation levels, as demonstrated by immunostaining. Fig. S3 shows that the number of inserted FKBP domains also positively correlates with EphB2 autophosphorylation as well as exogenous substrate phosphorylation as demonstrated by Western blot. Fig. S4 shows that dimerizer-induced Eph clustering is sufficient to trigger cellular responses such as EphB2 receptor internalization and EphB2- or EphA4-mediated cell collapse. Fig. S5 shows that N-terminally truncated EphB2 receptors are authophosphorylated and elicit cell collapse upon addition of the dimerizer, similar to the full-length isoforms, and that intracellular clustering of EphB2 changes the sensitivity of cells toward extracellular ephrinB2-Fc. Video 1 shows that fluorescent anisotropy in cells transfected with kdEphB2-3FKBP clearly decreases upon application of the dimerizer, indicative of receptor clustering. Video 2 shows the typical cell collapse and respreading response of an EphB2-3FKBP transfected cell stimulated with

the dimerizer. Online supplemental material is available at http://www.jcb.org/cgi/content/full/jcb.201305037/DC1.

References

Astin, J.W., J. Batson, S. Kadir, J. Charlet, R.A. Persad, D. Gillatt, J.D. Oxley, and C.D. Nobes. 2010. Competition amongst Eph receptors regulates contact inhibition of locomotion and invasiveness in prostate cancer cells. *Nat. Cell Biol.* 12:1194–1204. http://dx.doi.org/10.1038/ncb2122

Carvalho, R.F., M. Beutler, K.J. Marler, B. Knöll, E. Becker-Barroso, R. Heintzmann, T. Ng, and U. Drescher. 2006. Silencing of EphA3 through a cis interaction with ephrinA5. *Nat. Neurosci.* 9:322–330. http://dx.doi.org/10.1038/nn1655

Chen, J., X.F. Zheng, E.J. Brown, and S.L. Schreiber. 1995. Identification of an 11-kDa FKBP12-rapamycin-binding domain within the 289-kDa FKBP12-rapamycin-associated protein and characterization of a critical serine residue. *Proc. Natl. Acad. Sci. USA.* 92:4947–4951. http://dx.doi.org/10.1073/pnas.92.11.4947

Choi, J., J. Chen, S.L. Schreiber, and J. Clardy. 1996. Structure of the FKBP12-rapamycin complex interacting with the binding domain of human FRAP. *Science.* 273:239–242. http://dx.doi.org/10.1126/science.273.5272.239

Clackson, T., W. Yang, L.W. Rozamus, M. Hatada, J.F. Amara, C.T. Rollins, L.F. Stevenson, S.R. Magari, S.A. Wood, N.L. Courage, et al. 1998. Redesigning an FKBP-ligand interface to generate chemical dimerizers with novel specificity. *Proc. Natl. Acad. Sci. USA.* 95:10437–10442. http://dx.doi.org/10.1073/pnas.95.18.10437

Davis, S., N.W. Gale, T.H. Aldrich, P.C. Maisonpierre, V. Lhotak, T. Pawson, M. Goldfarb, and G.D. Yancopoulos. 1994. Ligands for EPH-related receptor tyrosine kinases that require membrane attachment or clustering for activity. *Science.* 266:816–819. http://dx.doi.org/10.1126/science.7973638

Dong, H., S. Qin, and H.-X. Zhou. 2010. Effects of macromolecular crowding on protein conformational changes. *PLOS Comput. Biol.* 6:e1000833. http://dx.doi.org/10.1371/journal.pcbi.1000833

Egea, J., and R. Klein. 2007. Bidirectional Eph-ephrin signaling during axon guidance. *Trends Cell Biol.* 17:230–238. http://dx.doi.org/10.1016/j.tcb.2007.03.004

Egea, J., U.V. Nissen, A. Dufour, M. Sahin, P. Greer, K. Kullander, T.D. Mrsic-Flogel, M.E. Greenberg, O. Kiehn, P. Vanderhaeghen, and R. Klein. 2005. Regulation of EphA 4 kinase activity is required for a subset of axon guidance decisions suggesting a key role for receptor clustering in Eph function. *Neuron.* 47:515–528. http://dx.doi.org/10.1016/j.neuron.2005.06.029

Gale, N.W., S.J. Holland, D.M. Valenzuela, A. Flenniken, L. Pan, T.E. Ryan, M. Henkemeyer, K. Strebhardt, H. Hirai, D.G. Wilkinson, et al. 1996. Eph receptors and ligands comprise two major specificity subclasses and are reciprocally compartmentalized during embryogenesis. *Neuron.* 17:9–19. http://dx.doi.org/10.1016/S0896-6273(00)80276-7

Grunwald, I.C., M. Korte, D. Wolfer, G.A. Wilkinson, K. Unsicker, H.P. Lipp, T. Bonhoeffer, and R. Klein. 2001. Kinase-independent requirement of EphB2 receptors in hippocampal synaptic plasticity. *Neuron.* 32:1027–1040. http://dx.doi.org/10.1016/S0896-6273(01)00550-5

Himanen, J.-P., M.J. Chumley, M. Lackmann, C. Li, W.A. Barton, P.D. Jeffrey, C. Vearing, D. Geleick, D.A. Feldheim, A.W. Boyd, et al. 2004. Repelling class discrimination: ephrin-A5 binds to and activates EphB2 receptor signaling. *Nat. Neurosci.* 7:501–509. http://dx.doi.org/10.1038/nn1237

Himanen, J.P., L. Yermekbayeva, P.W. Janes, J.R. Walker, K. Xu, L. Atapattu, K.R. Rajashankar, A. Mensinga, M. Lackmann, D.B. Nikolov, and S. Dhe-Paganon. 2010. Architecture of Eph receptor clusters. *Proc. Natl. Acad. Sci. USA.* 107:10860–10865. http://dx.doi.org/10.1073/pnas.1004148107

Hofman, E.G., A.N. Bader, J. Voortman, D.J. van den Heuvel, S. Sigismund, A.J. Verkleij, H.C. Gerritsen, and P.M. van Bergen en Henegouwen. 2010. Ligand-induced EGF receptor oligomerization is kinase-dependent and enhances internalization. *J. Biol. Chem.* 285:39481–39489. http://dx.doi.org/10.1074/jbc.M110.164731

Holmberg, J., D.L. Clarke, and J. Frisén. 2000. Regulation of repulsion versus adhesion by different splice forms of an Eph receptor. *Nature*. 408:203–206. http://dx.doi.org/10.1038/35041577

Janes, P.W., E. Nievergall, and M. Lackmann. 2012. Concepts and consequences of Eph receptor clustering. *Semin. Cell Dev. Biol.* 23:43–50. http://dx.doi.org/10.1016/j.semcdb.2012.01.001

Kayser, M.S., A.C. McClelland, E.G. Hughes, and M.B. Dalva. 2006. Intracellular and trans-synaptic regulation of glutamatergic synaptogenesis by EphB receptors. *J. Neurosci.* 26:12152–12164. http://dx.doi.org/10.1523/JNEUROSCI.3072-06.2006

Klein, R. 2009. Bidirectional modulation of synaptic functions by Eph/ephrin signaling. *Nat. Neurosci.* 12:15–20. http://dx.doi.org/10.1038/nn.2231

Lauterbach, J., and R. Klein. 2006. Release of full-length EphB2 receptors from hippocampal neurons to cocultured glial cells. *J. Neurosci.* 26:11575–11581. http://dx.doi.org/10.1523/JNEUROSCI.2697-06.2006

Lemmon, M.A., and J. Schlessinger. 2010. Cell signaling by receptor tyrosine kinases. *Cell*. 141:1117–1134. http://dx.doi.org/10.1016/j.cell.2010.06.011

Lim, B.K., N. Matsuda, and M.M. Poo. 2008. Ephrin-B reverse signaling promotes structural and functional synaptic maturation in vivo. *Nat. Neurosci.* 11:160–169. http://dx.doi.org/10.1038/nn2033

Marquardt, T., R. Shirasaki, S. Ghosh, S.E. Andrews, N. Carter, T. Hunter, and S.L. Pfaff. 2005. Coexpressed EphA receptors and ephrin-A ligands mediate opposing actions on growth cone navigation from distinct membrane domains. *Cell*. 121:127–139. http://dx.doi.org/10.1016/j.cell.2005.01.020

Muthuswamy, S.K., M. Gilman, and J.S. Brugge. 1999. Controlled dimerization of ErbB receptors provides evidence for differential signaling by homo- and heterodimers. *Mol. Cell. Biol.* 19:6845–6857.

Park, E.K., N. Warner, Y.S. Bong, D. Stapleton, R. Maeda, T. Pawson, and I.O. Daar. 2004. Ectopic EphA4 receptor induces posterior protrusions via FGF signaling in *Xenopus* embryos. *Mol. Biol. Cell*. 15:1647–1655. http://dx.doi.org/10.1091/mbc.E03-09-0674

Pasquale, E.B. 2008. Eph-ephrin bidirectional signaling in physiology and disease. *Cell*. 133:38–52. http://dx.doi.org/10.1016/j.cell.2008.03.011

Qiao, F., and J.U. Bowie. 2005. The many faces of SAM. *Sci. STKE*. 2005:re7.

Rohani, N., L. Canty, O. Luu, F. Fagotto, and R. Winklbauer. 2011. EphrinB/EphB signaling controls embryonic germ layer separation by contact-induced cell detachment. *PLoS Biol.* 9:e1000597. http://dx.doi.org/10.1371/journal.pbio.1000597

Runnels, L.W., and S.F. Scarlata. 1995. Theory and application of fluorescence homotransfer to melittin oligomerization. *Biophys. J.* 69:1569–1583. http://dx.doi.org/10.1016/S0006-3495(95)80030-5

Salaita, K., P.M. Nair, R.S. Petit, R.M. Neve, D. Das, J.W. Gray, and J.T. Groves. 2010. Restriction of receptor movement alters cellular response: physical force sensing by EphA2. *Science*. 327:1380–1385. http://dx.doi.org/10.1126/science.1181729

Seiradake, E., K. Harlos, G. Sutton, A.R. Aricescu, and E.Y. Jones. 2010. An extracellular steric seeding mechanism for Eph-ephrin signaling platform assembly. *Nat. Struct. Mol. Biol.* 17:398–402. http://dx.doi.org/10.1038/nsmb.1782

Seiradake, E., A. Schaupp, D. del Toro Ruiz, R. Kaufmann, N. Mitakidis, K. Harlos, A.R. Aricescu, R. Klein, and E.Y. Jones. 2013. Structurally encoded intraclass differences in EphA clusters drive distinct cell responses. *Nat. Struct. Mol. Biol.* 20:958–964. http://dx.doi.org/10.1038/nsmb.2617

Squire, A., P.J. Verveer, O. Rocks, and P.I. Bastiaens. 2004. Red-edge anisotropy microscopy enables dynamic imaging of homo-FRET between green fluorescent proteins in cells. *J. Struct. Biol.* 147:62–69. http://dx.doi.org/10.1016/j.jsb.2003.10.013

Stein, E., A.A. Lane, D.P. Cerretti, H.O. Schoecklmann, A.D. Schroff, R.L. Van Etten, and T.O. Daniel. 1998. Eph receptors discriminate specific ligand oligomers to determine alternative signaling complexes, attachment, and assembly responses. *Genes Dev.* 12:667–678. http://dx.doi.org/10.1101/gad.12.5.667

Varma, R., and S. Mayor. 1998. GPI-anchored proteins are organized in submicron domains at the cell surface. *Nature*. 394:798–801. http://dx.doi.org/10.1038/29563

Vearing, C., F.T. Lee, S. Wimmer-Kleikamp, V. Spirkoska, C. To, C. Stylianou, M. Spanevello, M. Brechbiel, A.W. Boyd, A.M. Scott, and M. Lackmann. 2005. Concurrent binding of anti-EphA3 antibody and ephrin-A5 amplifies EphA3 signaling and downstream responses: potential as EphA3-specific tumor-targeting reagents. *Cancer Res.* 65:6745–6754. http://dx.doi.org/10.1158/0008-5472.CAN-05-0758

Wang, L., R. Klein, B. Zheng, and T. Marquardt. 2011. Anatomical coupling of sensory and motor nerve trajectory via axon tracking. *Neuron*. 71:263–277. http://dx.doi.org/10.1016/j.neuron.2011.06.021

Whitney, M.L., K.G. Otto, C.A. Blau, H. Reinecke, and C.E. Murry. 2001. Control of myoblast proliferation with a synthetic ligand. *J. Biol. Chem.* 276:41191–41196. http://dx.doi.org/10.1074/jbc.M103191200

Wiesner, S., L.E. Wybenga-Groot, N. Warner, H. Lin, T. Pawson, J.D. Forman-Kay, and F. Sicheri. 2006. A change in conformational dynamics underlies the activation of Eph receptor tyrosine kinases. *EMBO J.* 25:4686–4696. http://dx.doi.org/10.1038/sj.emboj.7601315

Wimmer-Kleikamp, S.H., P.W. Janes, A. Squire, P.I.H. Bastiaens, and M. Lackmann. 2004. Recruitment of Eph receptors into signaling clusters does not require ephrin contact. *J. Cell Biol.* 164:661–666. http://dx.doi.org/10.1083/jcb.200312001

Wittig, I., H.P. Braun, and H. Schägger. 2006. Blue native PAGE. *Nat. Protoc.* 1:418–428. http://dx.doi.org/10.1038/nprot.2006.62

Wybenga-Groot, L.E., B. Baskin, S.H. Ong, J. Tong, T. Pawson, and F. Sicheri. 2001. Structural basis for autoinhibition of the Ephb2 receptor tyrosine kinase by the unphosphorylated juxtamembrane region. *Cell*. 106:745–757. http://dx.doi.org/10.1016/S0092-8674(01)00496-2

Yang, W., T.P. Keenan, L.W. Rozamus, X. Wang, V.M. Rivera, C.T. Rollins, T. Clackson, and D.A. Holt. 2003. Regulation of gene expression by synthetic dimerizers with novel specificity. *Bioorg. Med. Chem. Lett.* 13:3181–3184. http://dx.doi.org/10.1016/S0960-894X(03)00707-8

Zimmer, M., A. Palmer, J. Köhler, and R. Klein. 2003. EphB-ephrinB bidirectional endocytosis terminates adhesion allowing contact mediated repulsion. *Nat. Cell Biol.* 5:869–878. http://dx.doi.org/10.1038/ncb1045